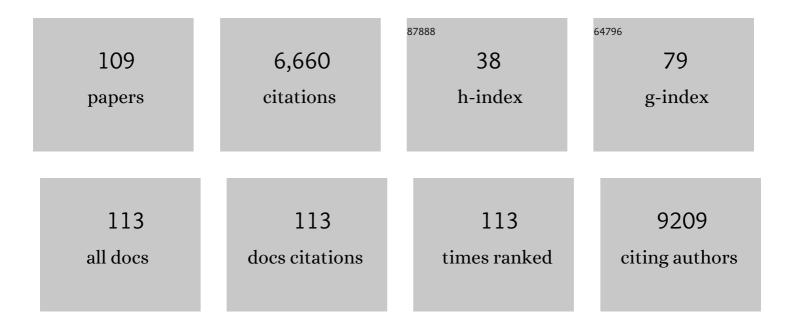
List of Publications by Year in descending order

Source: https://exaly.com/author-pdf/3067370/publications.pdf Version: 2024-02-01



XUEDONC BAL

#	Article	IF	CITATIONS
1	Chirality-specific growth of single-walled carbon nanotubes on solid alloy catalysts. Nature, 2014, 510, 522-524.	27.8	677
2	Rational design of layered oxide materials for sodium-ion batteries. Science, 2020, 370, 708-711.	12.6	616
3	Epitaxial growth of a 100-square-centimetre single-crystal hexagonal boron nitride monolayer on copper. Nature, 2019, 570, 91-95.	27.8	422
4	Arrays of horizontal carbon nanotubes of controlled chirality grown using designed catalysts. Nature, 2017, 543, 234-238.	27.8	317
5	Oxygen-Assisted Chemical Vapor Deposition Growth of Large Single-Crystal and High-Quality Monolayer MoS ₂ . Journal of the American Chemical Society, 2015, 137, 15632-15635.	13.7	301
6	Measuring the Work Function at a Nanobelt Tip and at a Nanoparticle Surface. Nano Letters, 2003, 3, 1147-1150.	9.1	257
7	Surface Doping to Enhance Structural Integrity and Performance of Liâ€Rich Layered Oxide. Advanced Energy Materials, 2018, 8, 1802105.	19.5	228
8	Revealing High Na-Content P2-Type Layered Oxides as Advanced Sodium-Ion Cathodes. Journal of the American Chemical Society, 2020, 142, 5742-5750.	13.7	206
9	Enabling Stable Cycling of 4.2 V Highâ€Voltage Allâ€Solidâ€State Batteries with PEOâ€Based Solid Electrolyte. Advanced Functional Materials, 2020, 30, 1909392.	14.9	204
10	An atlas of carbon nanotube optical transitions. Nature Nanotechnology, 2012, 7, 325-329.	31.5	186
11	Significantly enhanced critical current densities in MgB2 tapes made by a scaleable nanocarbon addition route. Applied Physics Letters, 2006, 88, 072502.	3.3	177
12	Self-adaptive strain-relaxation optimization for high-energy lithium storage material through crumpling of graphene. Nature Communications, 2014, 5, 4565.	12.8	139
13	Growing Zigzag (16,0) Carbon Nanotubes with Structure-Defined Catalysts. Journal of the American Chemical Society, 2015, 137, 8688-8691.	13.7	118
14	Seeded growth of large single-crystal copper foils with high-index facets. Nature, 2020, 581, 406-410.	27.8	116
15	Multidimensional Synergistic Nanoarchitecture Exhibiting Highly Stable and Ultrafast Sodiumâ€lon Storage. Advanced Materials, 2018, 30, e1707122.	21.0	112
16	Electrically Driven Redox Process in Cerium Oxides. Journal of the American Chemical Society, 2010, 132, 4197-4201.	13.7	101
17	Water-Assisted Preparation of High-Purity Semiconducting (14,4) Carbon Nanotubes. ACS Nano, 2017, 11, 186-193.	14.6	100
18	Optical fibres with embedded two-dimensional materials for ultrahigh nonlinearity. Nature Nanotechnology, 2020, 15, 987-991.	31.5	94

#	Article	IF	CITATIONS
19	Carbonâ€Doped Boron Nitride Nanosheets with Ferromagnetism above Room Temperature. Advanced Functional Materials, 2014, 24, 5985-5992.	14.9	86
20	A Single‣tep Hydrothermal Route to 3D Hierarchical Cu ₂ O/CuO/rGO Nanosheets as Highâ€Performance Anode of Lithiumâ€ion Batteries. Small, 2018, 14, 1702667.	10.0	84
21	Kinetic modulation of graphene growth by fluorine through spatially confined decomposition of metal fluorides. Nature Chemistry, 2019, 11, 730-736.	13.6	82
22	Highly Stable and Spectrally Tunable Gamma Phase Rb <i>_x</i> Cs _{1–} <i>_x</i> PbI ₃ Gradientâ€Alloyed Quantum Dots in PMMA Matrix through A Sites Engineering. Advanced Functional Materials, 2021, 31, 2008211.	14.9	73
23	Lattice Dynamics, Phonon Chirality, and Spin–Phonon Coupling in 2D Itinerant Ferromagnet Fe ₃ GeTe ₂ . Advanced Functional Materials, 2019, 29, 1904734.	14.9	70
24	Systematic determination of absolute absorption cross-section of individual carbon nanotubes. Proceedings of the National Academy of Sciences of the United States of America, 2014, 111, 7564-7569.	7.1	69
25	The Mechanistic Insights into the 2Hâ€IT Phase Transition of MoS ₂ upon Alkali Metal Intercalation: From the Study of Dynamic Sodiation Processes of MoS ₂ Nanosheets. Advanced Materials Interfaces, 2017, 4, 1700171.	3.7	65
26	Unusual role of epilayer–substrate interactions in determining orientational relations in van der Waals epitaxy. Proceedings of the National Academy of Sciences of the United States of America, 2014, 111, 16670-16675.	7.1	64
27	Gate-dependent pseudospin mixing in graphene/boron nitride moiré superlattices. Nature Physics, 2014, 10, 743-747.	16.7	64
28	Gluing Carbon Black and Sulfur at Nanoscale: A Polydopamineâ€Based "Nanoâ€Binder―for Double‧helled Sulfur Cathodes. Advanced Energy Materials, 2017, 7, 1601591.	19.5	64
29	Rolling Up a Monolayer MoS ₂ Sheet. Small, 2016, 12, 3770-3774.	10.0	60
30	Vertical graphene growth on uniformly dispersed sub-nanoscale SiO _x /N-doped carbon composite microspheres with a 3D conductive network and an ultra-low volume deformation for fast and stable lithium-ion storage. Journal of Materials Chemistry A, 2020, 8, 3822-3833.	10.3	59
31	In Situ Oxygen Doping of Monolayer MoS ₂ for Novel Electronics. Small, 2020, 16, e2004276.	10.0	54
32	Creating polar antivortex in PbTiO3/SrTiO3 superlattice. Nature Communications, 2021, 12, 2054.	12.8	50
33	Atomic imaging of mechanically induced topological transition of ferroelectric vortices. Nature Communications, 2020, 11, 1840.	12.8	49
34	Diffusion-controlled alloying of single-phase multi-principal transition metal carbides with high toughness and low thermal diffusivity. Applied Physics Letters, 2019, 114, .	3.3	48
35	Optical visualization and polarized light absorption of the single-wall carbon nanotube to verify intrinsic thermal applications. Light: Science and Applications, 2015, 4, e318-e318.	16.6	43
36	Strong Coupling between ZnO Excitons and Localized Surface Plasmons of Silver Nanoparticles Studied by STEM-EELS. Nano Letters, 2015, 15, 5926-5931.	9.1	42

XUEDONG BAI

#	Article	IF	CITATIONS
37	Robust growth of two-dimensional metal dichalcogenides and their alloys by active chalcogen monomer supply. Nature Communications, 2022, 13, 1007.	12.8	42
38	Atomic-scale observations of electrical and mechanical manipulation of topological polar flux closure. Proceedings of the National Academy of Sciences of the United States of America, 2020, 117, 18954-18961.	7.1	41
39	Layer-by-layer epitaxy of multi-layer MoS2 wafers. National Science Review, 2022, 9, .	9.5	41
40	Unraveling nanoscale electrochemical dynamics of graphite fluoride by <i>in situ</i> electron microscopy: key difference between lithiation and sodiation. Journal of Materials Chemistry A, 2020, 8, 6105-6111.	10.3	40
41	Synthesis of Carbon/Carbon Core/Shell Nanotubes with a High Specific Surface Area. Journal of Physical Chemistry C, 2009, 113, 61-68.	3.1	39
42	Valley Pseudospin with a Widely Tunable Bandgap in Doped Honeycomb BN Monolayer. Nano Letters, 2017, 17, 2079-2087.	9.1	37
43	In situ separator modification via CVD-derived N-doped carbon for highly reversible Zn metal anodes. Nano Research, 2022, 15, 9785-9791.	10.4	36
44	In Situ Imaging of On-Surface, Solvent-Free Molecular Single-Crystal Growth. Journal of the American Chemical Society, 2015, 137, 4972-4975.	13.7	35
45	Resistive switching mechanism in the one diode-one resistor memory based on p+-Si/n-ZnO heterostructure revealed by in-situ TEM. Scientific Reports, 2017, 7, 45143.	3.3	35
46	Intrinsic radial breathing oscillation in suspended single-walled carbon nanotubes. Physical Review B, 2011, 83, .	3.2	34
47	Evidence for electric-field-driven migration and diffusion of oxygen vacancies in Pr0.7Ca0.3MnO3. Journal of Applied Physics, 2012, 111, .	2.5	34
48	Cationâ€Deficiencyâ€Dependent CO ₂ Electroreduction over Copperâ€Based Ruddlesden–Popper Perovskite Oxides. Angewandte Chemie - International Edition, 2022, 61, .	13.8	33
49	Giant anisotropic photonics in the 1D van der Waals semiconductor fibrous red phosphorus. Nature Communications, 2021, 12, 4822.	12.8	32
50	Subunit cell–level measurement of polarization in an individual polar vortex. Science Advances, 2019, 5, eaav4355.	10.3	31
51	Regulation of phase transition and magnetocaloric effect by ferroelectric domains in FeRh/PMN-PT heterojunctions. Acta Materialia, 2020, 191, 51-59.	7.9	31
52	Filament growth dynamics in solid electrolyte-based resistive memories revealed by in situ TEM. Nano Research, 2014, 7, 1065-1072.	10.4	30
53	Facile Synthesis of Largeâ€Area Ultrathin Hexagonal BN Films via Selfâ€Limiting Growth at the Molten B ₂ O ₃ Surface. Small, 2013, 9, 1353-1358.	10.0	28
54	Realâ€ŧime Observation of Deep Lithiation of Tungsten Oxide Nanowires by Inâ€Situ Electron Microscopy. Angewandte Chemie - International Edition, 2015, 54, 15222-15225.	13.8	28

#	Article	IF	CITATIONS
55	Constructing Naâ€ion Cathodes via Alkali‧ite Substitution. Advanced Functional Materials, 2020, 30, 1910840.	14.9	28
56	In-situ TEM investigation of MoS2 upon alkali metal intercalation. Science China Chemistry, 2018, 61, 222-227.	8.2	26
57	Carbon nanotube transistors with graphene oxide films as gate dielectrics. Science China: Physics, Mechanics and Astronomy, 2010, 53, 828-833.	5.1	23
58	Real-time in situ TEM studying the fading mechanism of tin dioxide nanowire electrodes in lithium ion batteries. Science China Technological Sciences, 2013, 56, 2630-2635.	4.0	23
59	Microscopic Kinetics Pathway of Salt Crystallization in Graphene Nanocapillaries. Physical Review Letters, 2021, 126, 136001.	7.8	22
60	Engineering polar vortex from topologically trivial domain architecture. Nature Communications, 2021, 12, 4620.	12.8	20
61	Electroforming and endurance behavior of Al/Pr0.7Ca0.3MnO3/Pt devices. Applied Physics Letters, 2011, 99, .	3.3	19
62	Measurement of complex optical susceptibility for individual carbon nanotubes by elliptically polarized light excitation. Nature Communications, 2018, 9, 3387.	12.8	18
63	Synthesis of Honeycomb‧tructured Beryllium Oxide via Graphene Liquid Cells. Angewandte Chemie - International Edition, 2020, 59, 15734-15740.	13.8	18
64	Complete structural characterization of single carbon nanotubes by Rayleigh scattering circular dichroism. Nature Nanotechnology, 2021, 16, 1073-1078.	31.5	18
65	Three-Dimensional Limit of Bulk Rashba Effect in Ferroelectric Semiconductor GeTe. Nano Letters, 2021, 21, 77-83.	9.1	17
66	Ultralong aligned single-walled carbon nanotubes on flexible fluorphlogopite mica for strain sensors. Nano Research, 2012, 5, 443-449.	10.4	16
67	Towards the controlled CVD growth of graphitic B–C–N atomic layer films: The key role of B–C delivery molecular precursor. Nano Research, 2016, 9, 1221-1235.	10.4	16
68	Manipulating the Ferroelectric Domain States and Structural Distortion in Epitaxial BiFeO ₃ Ultrathin Films via Bi Nonstoichiometry. ACS Applied Materials & Interfaces, 2018, 10, 43792-43801.	8.0	15
69	Strain-Inhibited Electromigration of Oxygen Vacancies in LaCoO ₃ . ACS Applied Materials & Interfaces, 2019, 11, 36800-36806.	8.0	15
70	Surface plasmon enhanced solar-blind photoresponse of Ga2O3 film with Ga nanospheres. Science China: Physics, Mechanics and Astronomy, 2018, 61, 1.	5.1	14
71	Engineering of atomic-scale flexoelectricity at grain boundaries. Nature Communications, 2022, 13, 216.	12.8	14
72	Recent development of studies on the mechanism of resistive memories in several metal oxides. Science China: Physics, Mechanics and Astronomy, 2013, 56, 2361-2369.	5.1	12

#	Article	IF	CITATIONS
73	Revealing Three Stages of DNA-Cisplatin Reaction by a Solid-State Nanopore. Scientific Reports, 2015, 5, 11868.	3.3	12
74	Atomic origin of spin-valve magnetoresistance at the SrRuO3 grain boundary. National Science Review, 2020, 7, 755-762.	9.5	12
75	Visualizing Anisotropic Oxygen Diffusion in Ceria under Activated Conditions. Physical Review Letters, 2020, 124, 056002.	7.8	12
76	Revealing the Electrochemical Lithiation Routes of CuO Nanowires by inâ€Situ TEM. ChemElectroChem, 2016, 3, 1296-1300.	3.4	11
77	In-situ TEM study of the dynamic behavior of the graphene-metal interface evolution under Joule heating. Science China Technological Sciences, 2016, 59, 1080-1084.	4.0	11
78	Ferroelectric Proximity Effect and Topological Hall Effect in SrRuO ₃ /BiFeO ₃ Multilayers. ACS Applied Materials & Interfaces, 2022, 14, 6194-6202.	8.0	11
79	Enhanced Performance of Δ <i>T</i> _{ad} upon Frequent Alternating Magnetic Fields in FeRh Alloys by Introducing Second Phases. ACS Applied Materials & Interfaces, 2022, 14, 18293-18301.	8.0	11
80	Lithiumâ€lon Batteries: A Singleâ€Step Hydrothermal Route to 3D Hierarchical Cu ₂ O/CuO/rGO Nanosheets as Highâ€Performance Anode of Lithiumâ€lon Batteries (Small 5/2018). Small, 2018, 14, 1870020.	10.0	10
81	Atomic-Scale Observation of Structure Transition from Brownmillerite to Infinite Layer in SrFeO _{2.5} Thin Films. Chemistry of Materials, 2021, 33, 3113-3120.	6.7	10
82	Raman spectra and phonon structures of BaGa4Se7 crystal. Communications Physics, 2020, 3, .	5.3	9
83	Direct Observation of Inner-Layer Inward Contractions of Multiwalled Boron Nitride Nanotubes upon in Situ Heating. Nanomaterials, 2018, 8, 86.	4.1	8
84	Emergence of Insulating Ferrimagnetism and Perpendicular Magnetic Anisotropy in 3d–5d Perovskite Oxide Composite Films for Insulator Spintronics. ACS Applied Materials & Interfaces, 2022, 14, 15407-15414.	8.0	8
85	Reversible Intercalation of Alâ€lons in Poly(3,4â€Ethylenedioxythiophene):Poly(4â€Styrenesulfonate) Electrode for Aqueous Electrochemical Capacitors with High Energy Density. Energy Technology, 2021, 9, 2001036.	3.8	7
86	Two-Dimensional Room-Temperature Giant Antiferrodistortive SrTiO3 at a Grain Boundary. Physical Review Letters, 2021, 126, 225702.	7.8	7
87	Atomic-scale imaging of the defect dynamics in ceria nanowires under heating by in situ aberration-corrected TEM. Science China Chemistry, 2019, 62, 1704-1709.	8.2	6
88	Electrically driven motion, destruction, and chirality change of polar vortices in oxide superlattices. Science China: Physics, Mechanics and Astronomy, 2022, 65, 1.	5.1	6
89	Enhanced critical field and anomalous metallic state in two-dimensional centrosymmetric <mmi:math xmlns:mml="http://www.w3.org/1998/Math/MathML"><mml:mrow><mml:mn>1</mml:mn><mml:msup><mml:n mathvariant="normal">W<mml:msub><mml:mi mathvariant="normal">S<mml:msub><mml:mi Del view = Decoupled and anomalous metallic state in two-dimensional centrosymmetric <mml:math mathvariant="normal">S<mml:msub><mml:mi Del view = Decoupled and anomalous metallic state in two-dimensional centrosymmetric <mml:msup><mml:m mathvariant="normal">S<mml:msub><mml:mi mathvariant="normal">S<mml:mn>2</mml:mn></mml:mi </mml:msub></mml:m </mml:msup></mml:mi </mml:msub></mml:math </mml:mi </mml:msub></mml:mi </mml:msub></mml:n </mml:msup></mml:mrow>.</mmi:math 	ni>T3.2	:mi> <mml:m 6</mml:m
90	Physical Review 8, 2022, 105, . Surface protonation and oxygen evolution activity of epitaxial La1â^'xSrxCoO3 thin films. Science China: Physics, Mechanics and Astronomy, 2020, 63, 1.	5.1	5

#	Article	IF	CITATIONS
91	Development of in situ optical spectroscopy with high temporal resolution in an aberration-corrected transmission electron microscope. Review of Scientific Instruments, 2021, 92, 013704.	1.3	5
92	Atomic-scale dynamics of the phase transition in bilayer PtSe ₂ . Journal of Materials Chemistry C, 2021, 9, 5261-5266.	5.5	5
93	Broadband Plasmonic NbN Photocatalysts for Enhanced Hydrogen Generation from Ammonia Borane under Visible–Near-Infrared Illumination. Journal of Physical Chemistry Letters, 2022, 13, 4220-4226.	4.6	5
94	Perpendicular magnetic anisotropy induced by La _{2/3} Sr _{1/3} MnO ₃ –YBaCo ₂ O _{5+δ} interlayer coupling. Journal Physics D: Applied Physics, 2021, 54, 185302.	2.8	4
95	Insight into long-period pattern by depth sectioning using aberration-corrected scanning transmission electron microscope. Ultramicroscopy, 2020, 209, 112885.	1.9	3
96	Edge-Enriched Large-Area Hexagonal BN Ultrathin Films with Enhanced Optical Second Harmonic Generation. Journal of Physical Chemistry Letters, 2021, 12, 9475-9480.	4.6	3
97	NANOMECHANICS OF INDIVIDUAL ZINC OXIDE NANOBELTS MEASURED BY IN SITU TRANSMISSION ELECTRON MICROSCOPY. International Journal of Nanoscience, 2006, 05, 951-958.	0.7	2
98	Platinum composite nanowires for ultrasensitive mass detection. Applied Physics Letters, 2017, 110, 143102.	3.3	2
99	Atomic origin of Ti-deficient dislocation in SrTiO3 bicrystals and their electronic structures. Journal of Applied Physics, 2019, 126, .	2.5	2
100	Photo-enhanced field electron emission of cadmium sulfide nanowires. Science China: Physics, Mechanics and Astronomy, 2011, 54, 1963-1966.	5.1	1
101	Strong Coupling between ZnO Exciton and Localized Surface Plasmon in Ag Nanoparticles Studied by STEM-EELS. Microscopy and Microanalysis, 2015, 21, 1685-1686.	0.4	1
102	Surface plasmon enhanced solar-blind photoresponse of Ga2O3 film with Ga nanospheres. , 2018, 61, 1.		1
103	Electrical, Optical and Ionic Probe inside Transmission Electron Microscope. Materials Research Society Symposia Proceedings, 2013, 1525, 1.	0.1	0
104	Comparison of Structural Analysis and Electrochemical Studies of C-Li4Ti5O12 and CNT-Li4Ti5O12 Nanocomposites particles used as Anode for Lithium Ion Battery. Materials Research Society Symposia Proceedings, 2013, 1541, 75701.	0.1	0
105	Dynamic Rate Mechanism of V2O5 Coated SnO 2 Nanowires for Lithium Ion Batteries Studied by in situ TEM. Microscopy and Microanalysis, 2015, 21, 1913-1914.	0.4	0
106	Unraveling the "Seesaw―Competition between the Electrically Driven Reduction and Reoxidation Processes in Ceria with Inâ€Situ Electron Microscopy. ChemCatChem, 2016, 8, 3326-3329.	3.7	0
107	STEM-EELS Evaluation of the Dependence of Localized Surface Plasmon Linewidth on the Size of Au Nanoparticles. Microscopy and Microanalysis, 2017, 23, 1554-1555.	0.4	0
108	Synthesis of Honeycomb‧tructured Beryllium Oxide via Graphene Liquid Cells. Angewandte Chemie, 2020, 132, 15864-15870.	2.0	0

#	Article	IF	CITATIONS
109	Cationâ€Deficiencyâ€Dependent CO2 Electroreduction over Copperâ€Based Ruddlesdenâ€Popper Perovskite Oxides. Angewandte Chemie, 2022, 134, e202111670.	2.0	ο